JAAS

ROYAL SOCIETY OF CHEMISTRY

PAPER

View Article Online
View Journal | View Issue

Cite this: *J. Anal. At. Spectrom.*, 2025, **40**, 2826

Feasibility study to evaluate composition and degradation of orichalcum ingots through combined XRF and VIS-SWIR reflectance mapping

Anna Galli,[a] Jacopo Orsilli, *[a] Adele Sassella, [a] Luisa Raimondo, [a] Simone Caglio,[a] Maria Luisa Saladino, [bc] Francesco Armetta, [bc] Mario Berrettoni,[d] Paolo Conti [d] and Eugenio Caponetti[b]

Non-invasive and multi-analytical approaches are crucial for analyzing cultural heritage artifacts, particularly for rare and fragile specimens that must be studied *in situ*. The disadvantage of non-invasive techniques is their lower sensitivity and the limited information that can be collected without sampling the artifact; however, they allow the collection of multiple data sets on the same specimen. Besides, non-invasive techniques can collect more sample points or even a map on the same artifact, getting information about the whole object, considering its inhomogeneities due to possible alterations, without being biased by the chosen points. In this work, we employ an integrated instrument capable of simultaneously acquiring X-ray fluorescence and reflectance mapping in the visible-short wave infrared range to analyze orichalcum powder samples, then discussing the results in comparison with the analysis carried out using both *in situ* non-invasive techniques and laboratory-based non-destructive methods. These reference samples, derived from ingots recovered from a 6th-century BC shipwreck discovered off the coast of Gela, serve as a controlled dataset to validate the performance of the combined mapping approach. The aim is to assess the potential of this dual-modality system, enabling a comprehensive, bulk, and surface, characterization for future *in situ* applications to the ingots to check and follow the surface degradation phenomena, without the need for sampling.

Received 18th June 2025
Accepted 6th August 2025

DOI: 10.1039/d5ja00241a

rsc.li/jaas

Introduction

The ancient world is full of enigmatic treasures and materials that have captivated the imagination of scholars and historians for centuries. Among these, orichalcum stands out as a legendary alloy with mythical qualities, mentioned in the works of ancient philosophers and historians such as Plato and Pliny the Elder.[1,2] Described as a metal gleaming with a reddish hue and possessing gold-like properties, orichalcum was produced by a process far from easy, requiring a long and challenging procedure; as a result, the archaeological findings of orichalcum are not abundant. Thus, even though orichalcum is a Cu–Zn alloy produced since the IV–III millennium BCE.[3,4] Recent archaeological expeditions have brought forth startling revelations: in 2015, a team of underwater archaeologists uncovered a trove of ancient ingots off the coast of Gela, in southern Sicily. The city, established in 689 BC by Doric colonists from Rhodes and Crete, became in VI century BCE one of the most important towns of Sicily and a major trading centre of the Mediterranean Sea.[5,6]

When such rare and valuable samples are discovered, selecting the most effective and least invasive analytical techniques is crucial to preserve the findings, while performing multiple complementary analyses on the same sample to better characterize the objects. Then, only in a second attempt, if necessary, invasive and destructive techniques can be applied to selected specimens.

X-ray fluorescence (XRF) and diffuse reflectance (DR) spectroscopy provide complementary information: the former enables a qualitative and quantitative elemental analysis of the sample, exploiting the photoelectric absorption that occurs in the X-ray energy region and the subsequent atomic relaxation through the emission of fluorescence X-rays. The latter, instead, is based on the absorption and reflection properties of materials when stimulated by electromagnetic radiation in the visible (VIS, 360–1000 nm) and short-wave infrared (SWIR, 1000–2500 nm) ranges. In the visible spectral region, the reflectance curve is mainly characterized by phenomena related to electronic transitions. In SWIR, the spectra result from energy absorption within the crystal lattice due to vibrational

[a]*Department of Material Science, University of Milano-Bicocca, Via Cozzi 55, I-20125 Milano, Italy. E-mail: jacopo.orsilli@unimib.it*

[b]*Department of Biological, Chemical and Pharmaceutical Sciences and Technologies (STEBICEF)-University of Palermo, Viale Delle Scienze, Bld. 17, Palermo I-90128, Italy*

[c]*Institute for Chemical and Physical Processes IPCF-Messina, CNR, Viale Ferdinando Stagno d'Alcontres 37, I-98158 Messina, Italy*

[d]*Department of Chemistry, University of Camerino, 62032, Camerino, Macerata, Italy*

states. The combination of XRF and DR has already proven helpful in characterizing metals and analysing corrosion products.[7–12]

In this paper, we explore the potential of a dual-modality system combining XRF and VIS-SWIR reflectance mapping to characterize orichalcum samples. The analysis is carried out on powdered reference materials derived from ancient ingots recovered from a 6th-century BC shipwreck discovered off the coast of Gela (Sicily, Italy), which had been previously investigated using both *in situ* non-invasive and laboratory-based destructive methods. By comparing the results obtained with this integrated approach to those from the other methods, we assess its reliability and accuracy, then validate the system for direct *in situ* applications on archaeological metal artifacts, offering a rapid and non-invasive method for comprehensive bulk and surface characterization.

We stress that both the XRF and the mapping are non-invasive analyses, even if in this paper they are applied to microsamples sampled from the original artefacts.

Materials and methods

The three orichalcum samples studied, M04, M019, and M035, are chips from drilling original ingots from the Gela shipwreck[5] and have been analysed using all the techniques. Even though the samples were analysed with non-invasive methods, due to their size and the purpose of the study, it was preferable not to move the entire objects. For this reason, only small chips of the ingots were taken by drilling, and brought to the laboratory.

Point XRF

Point XRF analyses have been performed with ARTAX-200 from Bruker. The X-ray tube has a Mo anode, and the source beam can be collimated down to 0.65 mm in diameter (area of 0.33 mm^2) and filtered with different transmission filters. A Peltier-cooled silicon drift detector (SDD) collects the fluorescence radiation; it has an area of 10 mm^2, a crystal thickness of 0.45 mm, and an energetic resolution of 150 eV at the Mn Kα line. A charge-coupled device camera records the sample and is employed to select the measurement spot. In conjunction with a laser spot and crosshairs on the video display, it ensures the reproducible settings of the measuring distance and location of the measured spot.

For each sample, we obtained a mean composition of the alloy through three measurements in different areas of the samples. Each specimen has been placed on a square sample holder printed in polymeric material, namely poly-lactic acid (PLA), to minimize emissions, ensuring that the thickness of the deposition is infinite for both primary and fluorescence radiation. The source has been filtered with a Zr foil (15 μm thick) to better monochromatize the primary spectrum. The tube voltage was set at 50 kV and the current intensity at 0.3 mA, ensuring a low dead time and low intensity sum peaks for a collection time of 180 s.

XRF quantitative analysis can be accurate only if the sample is infinitely thick for the considered radiation and if the surface roughness is lower than the incoming wavelength.[13,14] For these reasons, we decided to perform preliminary tests to evaluate whether we can neglect the errors introduced by the sample morphology. We analysed a brass reference whose nominal composition is 5% Ni, 75% Cu, and 20% Zn. After analysing the brass, a reference was drilled to obtain a powder compatible with the orichalcum samples, and we analysed it using the same instrument under the same conditions. We recorded three measurements on both the reference and the drilled powder. As the error given by the sample preparation is lower than the quantification error, we could proceed with the quantitative analysis of the samples. The spectrum fitting and the concentration estimate were performed using QXAS software (IAEA).[15] We performed the quantitative analysis using the full fundamental parameters method, calibrated with reference metal samples whose composition is similar to that expected from the samples.

Diffuse reflectance

DR spectra were collected in the ultraviolet (UV)-vis-SWIR range (250–2500 nm) with a 1 nm step by using a PerkinElmer Lambda 1050 spectrometer, equipped with a 10 cm integrating sphere; thanks to home-made sample holders, which permit to probe only the sample and where the orichalcum is covered by a silica plate to fix it, the samples were mounted on one of the sphere ports to collect the total reflected light (diffuse + specular). The full reproducibility of the measurements was verified, and proper background correction was performed using a reference sample. The reference material, as well as the coating material of the sphere, is Spectralon.

Combined XRF and reflectance spectroscopy mapping

The combined system IRIS Bruker[16] is employed for non-destructive and non-contact analysis of the samples, allowing both single-point measurements and continuous scanning analysis. The measuring head combines an Energy Dispersive XRF (EDXRF) system, consisting of an X-ray tube, an SDD detector, a collimator, a filter wheel, and an optical system composed of optical fibres for VIS-SWIR spectroscopy.

The XRF head is equipped with a Rh transmission tube (anode thickness 1 μm), with a maximum power of 10 W, covered with a 250 μm thick Be window, and an SDD detector (active area of 50 mm^2, thickness 450 μm, resolution of approximately 138 eV at Mn K_α line) protected by a 12.5 μm thick Be window. The XRF mapping measurements were performed with a voltage of 40 kV and an intensity of 0.1 mA; the unfiltered source beam was collimated using a circular collimator with a diameter of 0.5 mm. The collection time for each point is 150 ms for a mapping speed of 0.6 mm s^{-1}.

The system for reflectance measurements consists of a halogen lamp with a nominal power of 9 mW, whose radiation is transported through a bundle of optical fibres to the head of the instrument and focused on the sample. The reflected light is then collected and transported by two different fibres of the same optical beam and sent to two spectrometers: one dedicated to the visible range (VIS 360–1000 nm with a resolution of

1.5 nm) and one to the infrared (SWIR 1000–2500 nm with a resolution of 8.9 nm). The white reference is a PTFE-based material; for black calibration, the instrument measures with the lamp shutter closed using the ambient lighting as a background reference. For an optimal measurement, it is best to carry out measurements in reduced or at least controlled light conditions; in this way, the background light radiation remains constant. Finally, a visible camera and a system with two lasers (axial and focus) are inserted into the head of the IRIS system for the correct positioning of the head in relation to the sample.

Quantitative analysis of the spectra was conducted using PyMCA software[17] and the built-in fundamental parameters quantification, utilizing a standard of copper to calculate the source flux.

Both for ARTAX and for IRIS, the intensity of Fe K_α has been corrected automatically by the software employed before the quantification due to the overlapping of the fluorescence line with the Cu K_α escape peak (energy difference of 0.1 keV).

Results and discussion

The XRF-mapping (MA-XRF) technique assesses the compositional homogeneity of the samples; using regions of interest, (ROIs) centred on the K_α of Cu, K_β line of Zn (to avoid overlapping with copper lines), and L_α line of Pb, we observed that the main elements are equally distributed, for all the samples, with a more intense signal of Cu and Zn and a lower intensity of Pb (causing the maps to show a yellowish hue in the central region of the samples). This is evident in Fig. 1, where the RGB images have been reconstructed from the elemental distribution of major elements.

Also, a homogenous variability in the signal intensity can be observed in different regions of the map due to the geometry of the samples in the form of chips, with an irregular surface. The higher intensity of the Pb signal at the border of the samples can be ascribed to border effects caused by the shapes of the chips. Indeed, we can observe that this effect is mostly present in the right border of the chips, suggesting that it is caused by the geometry of detection and irradiation.

Starting from the map of copper, the average XRF spectra for each sample can be calculated as the average of all the spectra collected, weighted for the copper K_α intensity. This choice was applied only because the samples were proven compositionally homogeneous; otherwise, an average mean calculated in this way would have resulted in a spectrum that mainly reflects the composition of the copper-rich areas.

The average spectra (Fig. 2) show the presence of trace elements on the tail of copper (Ti, Cr, Mn, and Ni); these spectra, therefore, allow for a very sensitive compositional even if the intensity of the signal of these elements is too low to obtain an accurate map of these elements.

The average spectra obtained from the whole map are also more suitable for comparing the overall composition of the samples and for observing differences in the average composition more clearly, when correctly normalized for the extent of the investigated area. Moreover, we can observe that the composition of the three samples is very similar, with a slight difference in the background intensity, due to the sample deposition on carbon tape, which is reflected in the signal intensity.

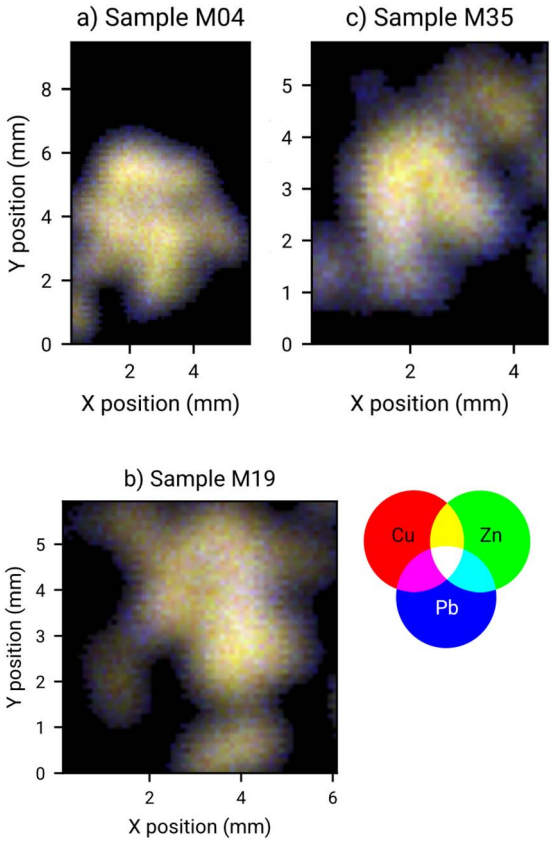

Fig. 1 RGB images obtained from the XRF spectra of the three samples: (a) sample M04, (b) sample M19, and (c) sample M35. In red is the signal of Cu, in green is the signal of Zn, and in blue is the signal of Pb.

By analysing the same samples with ARTAX spectrometer, we first tested the homogeneity of samples: XRF spectra collected in three different areas for all samples (Fig. 3) show a homogeneous material composition, as the intensity observed is very similar. The only elements detected are Cu, Zn, Pb, Fe, and traces of Ni; indeed, the high-intensity tail of copper, caused by incomplete charge collection in the detector crystal, increases the background at low energies, hindering the possibility of detection of trace elements lighter than copper itself. We can observe that the intensity of the background of the sample M04 is lower for higher energy, and the Compton peak is lower. This is due to the sample deposition over the PLA sample holder; for this sample, a higher amount of sample volume has been irradiated, causing a lower diffusion from PLA and a slightly higher intensity of the fluorescence peaks.

To perform a precise comparison between the two instruments, IRIS and ARTAX, spectra collected with them on the same sample, M35, are reported in Fig. 4. We can observe that the signal obtained with IRIS is higher, and we have a lower (in proportion) contribution of the scattering, and we can detect better elements present in lower concentration. However, Mo excitation is close in energy to the absorption edges of the

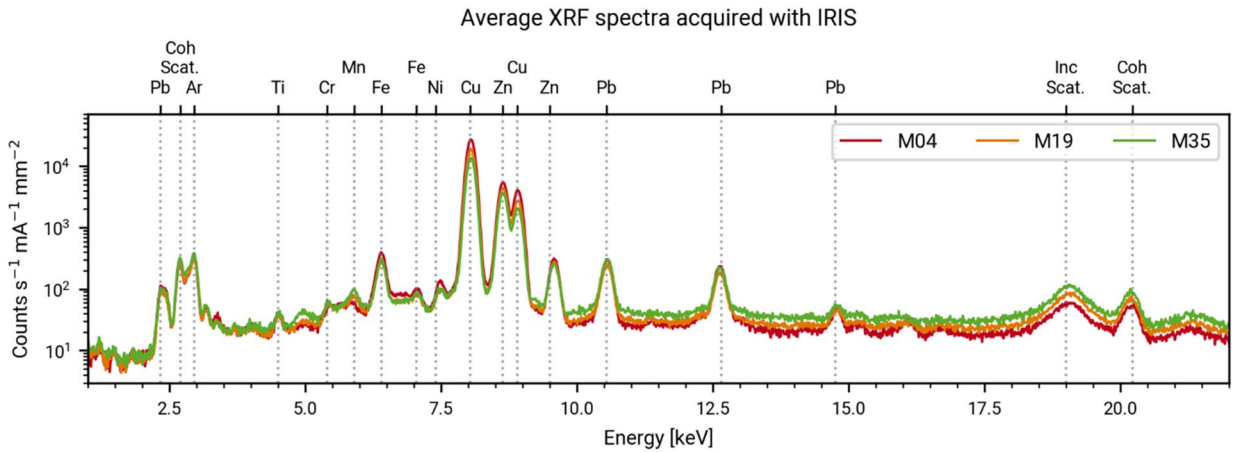

Fig. 2 Average XRF spectra acquired with IRIS of the three samples, elements at lower energies can be better resolved; the peaks observed are marked. The spectra are normalized for the tube current, the measurement live time and the investigated area.

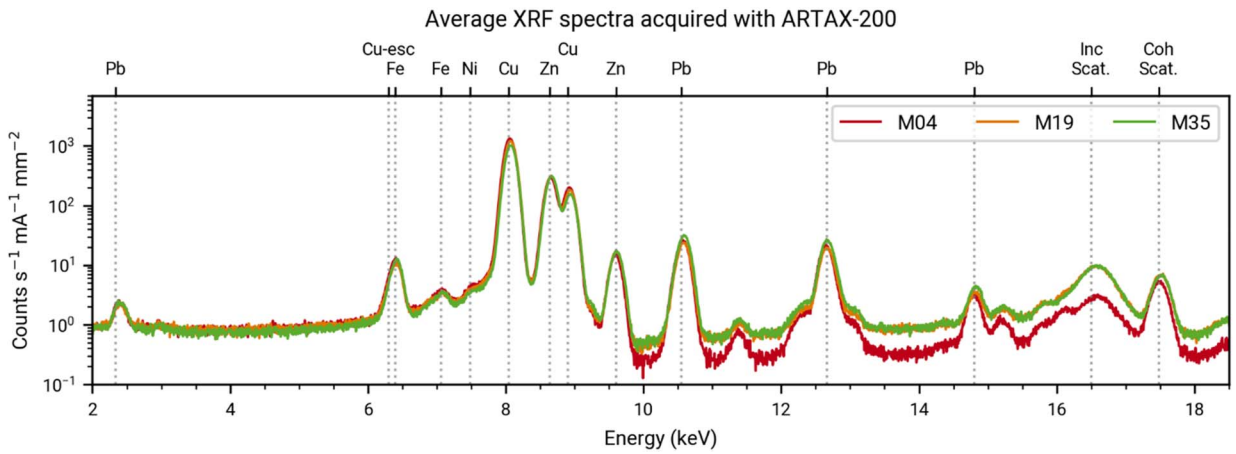

Fig. 3 Normalized average XRF spectra collected on the three samples. The spectra are normalized for the tube current, the measurement live time and the investigated area. The peaks observed are marked. For sample M04 the diffusion background is lower as less signal form the plastic substrate was collected.

elements of interest; thus, we observe a higher intensity of the fluorescence lines, compared with the spectra collected with a Rh anode.

After validating the qualitative analysis obtained using the two different EDXRF instruments, ARTAX and IRIS, the collected data are then used here to get the quantitative analysis

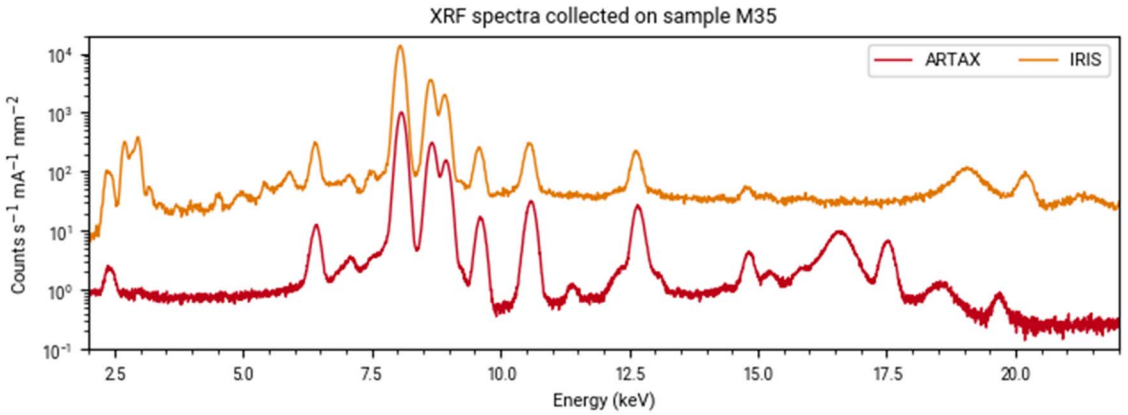

Fig. 4 Comparison between spectra collected with ARTAX and IRIS on the sample M35.

Table 1 Results of the quantitative analysis performed with ARTAX and IRIS on the orichalcum samples. For each element, the error is expressed as the last digit. Elements not detected are indicated as u.d.l. (under detection limit)

Instr.	Sample	Ti ppm	Cr ppm	Mn ppm	Fe ppm	Ni[a] ppm	Cu [%]	Zn [%]	Pb [%]
ARTAX	M04	u.d.l.	u.d.l.	u.d.l.	4124(88)	498(39)	80.4(4)	14.2(2)	5.0(4)
	M19	u.d.l.	u.d.l.	u.d.l.	3611(40)	466(31)	78.5(6)	16.1(1)	5.0(6)
	M35	u.d.l.	u.d.l.	u.d.l.	5218(105)	484(27)	73.8(4)	19(1)	7(2)
IRIS	M04	1091(44)	672(28)	486(25)	5759(47)	1362(35)[a]	80.1(1)	14.5(1)	4.5(1)
	M19	1267(59)	941(41)	1161(40)	5610(57)	1047(42)[a]	77.7(1)	16.4(1)	4.9(1)
	M35	1721(107)	1244(75)	2171(77)	8308(102)	1442(72)[a]	73.0(1)	18.1(1)	7.4(1)

[a] Overestimated (see text).

of the alloys, reported in Table 1. The data from ARTAX are the average concentrations of three measures (in ppm for Fe, and w% for Cu, Zn, and Pb) with their standard deviations; IRIS data and their standard deviation have been calculated from the average spectra obtained from the whole map spectra.

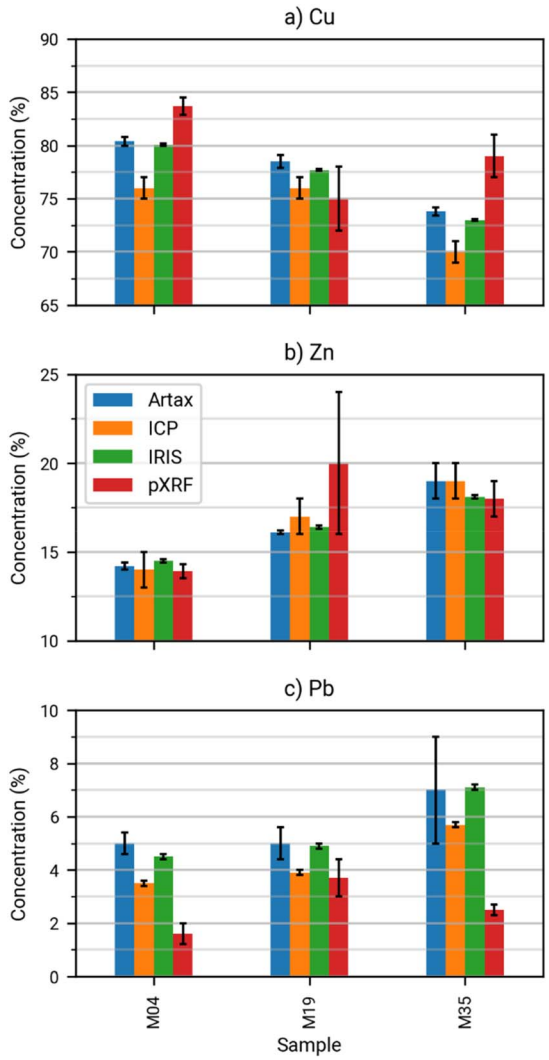

Fig. 5 Comparison between the obtained data and the published data of (a) copper, (b) zinc, and (c) lead.[5,18]

The results obtained with the two spectrometers agree, with an average Cu concentration of around 77% and an average Zn concentration of 16%. With IRIS, it has also been possible to quantify elements at lower Z, like Ti, Cr, and Mn, undetectable with ARTAX; however, we can observe that IRIS provides a critical overestimation of Ni (3–4 times higher) due to the presence of a Ni collimator, which makes it impossible to quantify trace concentrations of this element.

Recently, the compositions of the same chips of orichalcum ingots have been already analysed by means of Inductively Coupled Plasma Optical Emission Spectroscopy (ICP-OES);[18] moreover, in a more extensive experimental campaign, the same researcher team has directly measured the alloy composition *in situ* by XRF with a portable instrument (p-XRF), without sampling by analysing the ingot and following the same methodology detailed in a previous study,[5] to ensure consistency in the analytical approach. In Fig. 5, the comparison between the published data, the pXRF campaign on the same batch of samples, and the data of the present work (reported in Table 1), is shown for the main components of the alloy.

The concentration values for Cu obtained with ARTAX and IRIS are in the range of those collected with ICP-OES and the p-XRF, where the former tend to represent the lower value and the latter the upper value, except for sample M19, where the data are almost compatible, considering the error bars. For Zn, the data are all well within the compositional range. Only for Pb we observe a slight overestimation, if we compare the IRIS data with the p-XRF ones, which can be ascribed to the use of the L_β line instead of the L_α line; a better compatibility is observed with the ICP-OES data.

In addition to analysing the orichalcum samples in terms of elemental composition, their diffuse reflectance was also analysed both with the IRIS integrated scanner used for mapping and with a laboratory-based benchtop system, with the aim of establishing a reliable reference dataset. Based on this comparison, the interpretation of future *in situ* analyses of the ingots in their conservation environments, where only non-invasive investigations are feasible, may be easier and more accurate.

Looking at the spectra acquired with IRIS, in Fig. 6 the data collected from the whole mapped surface, obtained by summing all the spectra in the selected spectral ranges, are shown. These data show the same band in the VIS range, attributed to the characteristic response of brass.[19] In the SWIR

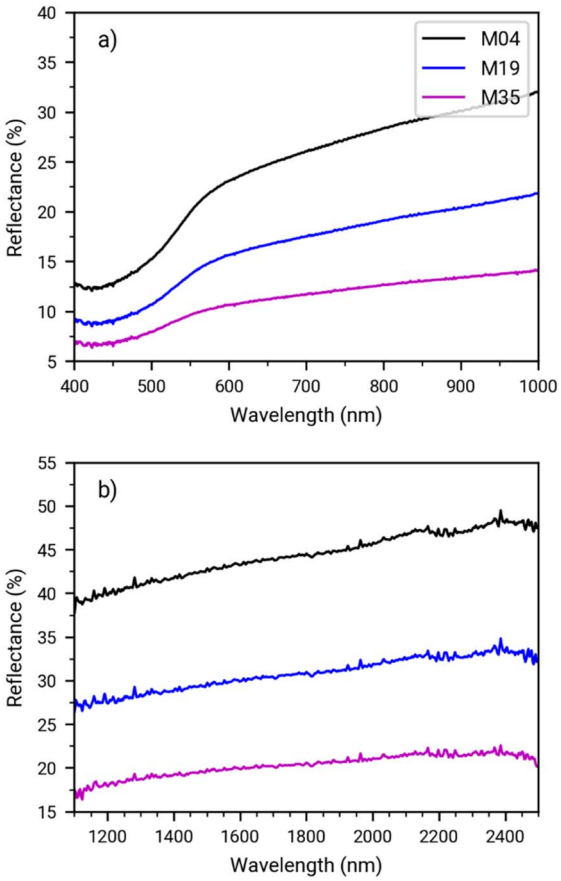

Fig. 6 RS spectra collected with IRIS, (a) in the UV-vis region, (b) in the SWIR region.

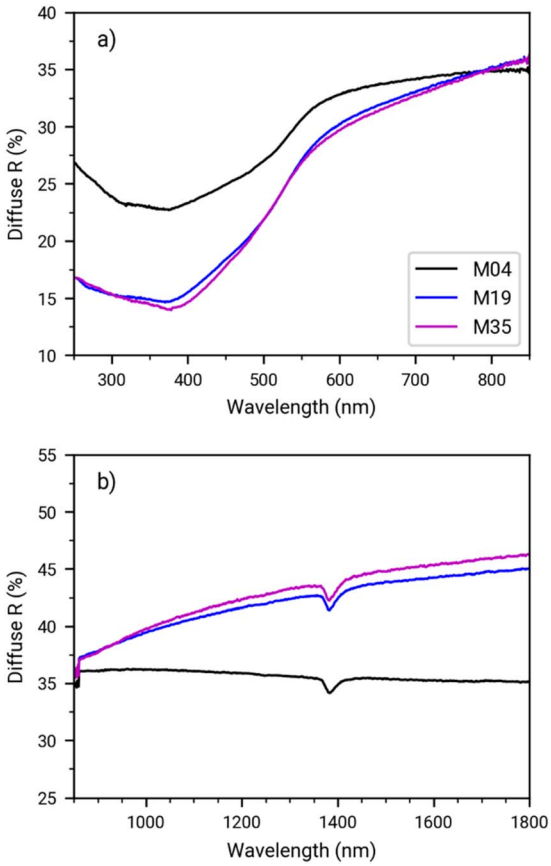

Fig. 7 Diffuse reflectance spectra of samples M04, M19, and M35 (black, blue, and pink curves, respectively) in the UV-vis spectral range (a) and in the SWIR spectral range (b).

range, although the spectra are noisy and although a contribution from the spectral correction with the white reference cannot be excluded *a priori*, in all the three samples an absorption band at 2250 nm can still be distinguished, which can suggest the presence of Fe–OH bonds, being similar to that observed in the spectra of chlorite structure in zinc–lead–silver deposit[20] and heavy metals in copper rich soils.[21] Even if this band is very weak, it could be interesting to measure the spectra from the degraded ingot surface, to check the possibility of using it for monitoring the evolution of degradation itself. Orsilli *et al.*,[7] by using IRIS scanner, already observed this absorption band in archaeological copper alloys, suggesting that monitoring in time the orichalcum response could track the progression of surface degradation, *e.g.* the dynamics of metallic iron oxidation into a compound containing FeOH groups. It should be noted that the surface of the orichalcum ingots, much different from the bulk samples studied here, is heavily corroded; this is clearly due to degradation of the alloy in sea water and (for much less time) in air, so that studying the surface *in situ* may add worthy information on the history of these artifacts.

DR in the UV-vis-SWIR spectral range has been measured on the three orichalcum samples using also the laboratory spectrometer. The results are reported in Fig. 7, where the spectra of samples M04, M19, and M35 are shown in the spectral ranges from 250 to 850 nm (a) and from 850 to 1800 nm (b). The spectra of the three orichalcum samples are very similar to each other, with a broad minimum from about 250 nm up to 600 nm, with peaks detectable at 315 nm and 375 nm and a shoulder at about 500 nm. The three samples look very similar upon direct inspection by eye and present similar compositions, all of them with Cu $\geq$ 70% and Zn $\leq$ 20%.

The UV-vis features of orichalcum originate from the d-bands corresponding to Cu and Zn states, at higher and lower energy, respectively, which give the typical reddish-gold colour of this alloy. In particular, the spectra in Fig. 6a show a very good match with the α-brass phase,[22] characterized by a Zn content below 37 at% as our samples. In the SWIR range in Fig. 6b, the response of all the orichalcum samples is featureless, with just a small peak at about 1380 nm from the silica plate used in the sample holder. At higher wavelength, up to 2500 nm (not shown), residual reflectance peaks from the silica plate and background correction prevent the detection of any possible response from orichalcum components, such as oxides and minerals (see, *e.g.*, ref. 9).

Conclusions

Orichalcum, the copper alloy famously described by Pliny and Plato, has been in production since the 4th–3rd millennium

BCE. In this study, we compared a non-invasive, multi-technique approach combining mapping-based methods (MA-XRF and reflectance spectroscopy mapping) with point-based techniques (XRF and diffuse reflectance), aiming to evaluate the capability of the mapping system to assess both bulk composition and surface conditions of archaeological metal artifacts.

It is well known that the integration of XRF spectroscopy and the visible – SWIR reflectance spectroscopy provided complementary information on elemental and molecular composition—particularly valuable in cultural heritage studies where corrosion and surface alterations are common. To validate the effectiveness of the mapping techniques, we compared the results with both point-based analyses and previously published compositional data obtained *via* other techniques on the same samples. The mapping data showed a good consistency with these reference datasets.

Our work demonstrates the potential of this mapping system to deliver reliable, spatially resolved information on both the alloy composition and surface degradation of ancient metallic artifacts. We propose its use *in situ* on orichalcum ingots with corroded surfaces, where MA-XRF can provide robust bulk compositional data, and reflectance spectroscopy mapping can reveal the spatial distribution of alteration products, offering a powerful, non-destructive tool for archaeological and conservation studies.

Author contributions

AG conceptualisation, JO, SC data curation, JO, SC, LR investigation, AG, AS methodology, FA, MLS, MB, PC, EC validation, AG, AS, JO writing – original draft, All the authors writing – review & editing.

Conflicts of interest

There are no conflicts to declare.

Data availability

Data for this article are available from the following online repository: Galli, Anna; Orsilli, Jacopo; Sassella, Adele; Raimondo, Luisa; Caglio, Simone; Saladino, Maria Luisa; Armetta, Francesco (2025), "Orichalcum Ingots dataset", Bicocca Open Archive Research Data, V2, doi: **https://www.doi.org/10.17632/tp526jcf8c.2**. **https://board.unimib.it/datasets/tp526jcf8c/2**.

Notes and references

1 Plato, *Critias*, 114a–116e.
2 Pliny the Elder, *Naturalis Historia*, ch. 2, vol. **XXXIV**.
3 P. T. Craddock, *J. Archaeol. Sci.*, 1978, **5**, 1–16.
4 R. J. Forbes, *Studies in Ancient Technology*, E.J. Brill, Leiden; New York, 1993.
5 E. Caponetti, F. Armetta, D. C. Martino, M. L. Saladino, S. Ridolfi, G. Chirco, M. Berrettoni, P. Conti, N. Bruno and S. Tusa, *Mediterr. Archaeol. Archaeom.*, 2017, **17**, 11–18, DOI: **10.5281/zenodo.581716**.
6 E. Caponetti, F. Armetta, L. Brusca, D. Chillura Martino, M. L. Saladino, S. Ridolfi, G. Chirco, M. Berrettoni, P. Conti, N. Bruno and S. Tusa, *Microchem. J.*, 2017, **135**, 163–170.
7 J. Orsilli and S. Caglio, *Minerals*, 2024, **14**, 192.
8 S. Bracci, S. Vettori, E. Cantisani, I. Degano and M. Galli, *Archaeol. Anthropol. Sci.*, 2019, **11**, 1611–1619.
9 E. Catelli, G. Sciutto, S. Prati, Y. Jia and R. Mazzeo, *Environ. Sci. Pollut. Res.*, 2018, **25**, 24379–24393.
10 E. Catelli, L. L. Randeberg, H. Strandberg, B. K. Alsberg, A. Maris and L. Vikki, *J. Spectr. Imaging*, 2018, **7**, DOI: **10.1255/jsi.2018.a10**.
11 L. Bonizzoni, A. Galli and G. Poldi, *X-Ray Spectrom.*, 2008, **37**, 388–394.
12 W. Liu, M. Li, N. Wu, S. Liu and J. Chen, *J. Cult. Herit.*, 2021, **49**, 19–27.
13 D. K. G. de Boer, *Phys. Rev. B:Condens. Matter Mater. Phys.*, 1994, **49**, 5817–5820.
14 C. Duée, B. Orberger, N. Maubec, V. Laperche, L. Capar, A. Bourguignon, X. Bourrat, Y. El Mendili, D. Chateigner, S. Gascoin, M. Le Guen, C. Rodriguez, F. Trotet, M. Kadar, K. Devaux, M. Ollier, H. Pillière, T. Lefèvre, D. Harang, F. Eijkelkamp, H. Nolte and P. Koert, *J. Geochem. Explor.*, 2019, **198**, 1–17.
15 P. Kregsamer, *QXAS – Quantitative X-Ray Analysis System (User's Manual and Guide to X-Ray Fluorescence Technique)*, IAEA, 2009.
16 M. Occhipinti, R. Alberti, T. Parsani, C. Dicorato, P. Tirelli, M. Gironda, A. Tocchio and T. Frizzi, *X-Ray Spectrom.*, 2024, **53**, 520–530.
17 V. A. Solé, E. Papillon, M. Cotte, Ph. Walter and J. Susini, *Spectrochim. Acta, Part B*, 2007, **62**, 63–68.
18 E. Caponetti, F. Armetta, L. Brusca, M. Ferrante, D. Chillura Martino, M. L. Saladino, D. Guastella, G. Chirco, M. Berrettoni, S. Zamponi, P. Conti and S. Tusa, *J. Archaeol. Sci.*, 2021, **37**, 102901.
19 M. Aceto, A. Agostino, G. Fenoglio, A. Idone, M. Gulmini, M. Picollo, P. Ricciardi and J. K. Delaney, *Anal. Methods*, 2014, **6**, 1488–1500.
20 Y. Sun, P. K. Seccombe and K. Yang, *J. Geochem. Explor.*, 2001, **73**, 11–26.
21 F. Yin, M. Wu, L. Liu, Y. Zhu, J. Feng, D. Yin, C. Yin and C. Yin, *Int. J. Appl. Earth Obs. Geoinf.*, 2021, **102**, 102420.
22 V. J. Keast, J. Ewald, K. S. B. De Silva, M. B. Cortie, B. Monnier, D. Cuskelly and E. H. Kisi, *J. Alloys Compd.*, 2015, **647**, 129–135.